AD-A221 330

Plasma Wave Observations During Ion Gun Experiments

R.C. OLSEN, and L.E. WEDDLE
Physics Department
Naval Postgraduate School
Monterey, CA 93943

and

J. L. ROEDER
Space Sciences Laboratory
Laboratory Operations
The Aerospace Corporation
El Segundo, CA 90245-4691
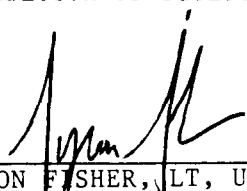
20 March 1990

Prepared for

SPACE SYSTEMS DIVISION
AIR FORCE SYSTEMS COMMAND
Los Angeles Air Force Base
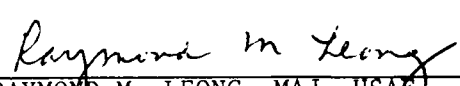P.O. Box 92960
Los Angeles, CA 90009-2960

This report was submitted by The Aerospace Corporation, El Segundo, CA 90245, under Contract No. F04701-88-C-0089 with the Space Systems Division, P.O. Box 92960, Los Angeles, CA 90009-2960. It was reviewed and approved for The Aerospace Corporation by H. R. Rugge, Director, Space Sciences Laboratory. Lt. T. Fisher was the project officer for the Mission-Oriented Investigation and Experimentation (MOIE) Program.

This report has been reviewed by the Public Affairs Office (PAS) and is releasable to the National Technical Information Service (NTIS). At NTIS, it will be available to the general public, including foreign nationals.

This technical report has been reviewed and is approved for publication. Publication of this report does not constitute Air Force approval of the report's findings or conclusions. It is published only for the exchange and stimulation of ideas.

TRYON FISHER, LT, USAF
MOIE Project Officer
SSD/CLFPO

RAYMOND M. LEONG, MAJ, USAF
MOIE Program Manager
AFSTC/WCO OL-AB

REPORT DOCUMENTATION PAGE

1a. REPORT SECURITY CLASSIFICATION Unclassified		1b. RESTRICTIVE MARKINGS
2a. SECURITY CLASSIFICATION AUTHORITY		3. DISTRIBUTION/AVAILABILITY OF REPORT Approved for public release; distribution unlimited.
2b. DECLASSIFICATION DOWNGRADING SCHEDULE		

4. PERFORMING ORGANIZATION REPORT NUMBER(S) TR-0089(4940-06)-6	5. MONITORING ORGANIZATION REPORT NUMBER(S) SSD-TR-90-014

6a. NAME OF PERFORMING ORGANIZATION The Aerospace Corporation Laboratory Operations	6b. OFFICE SYMBOL (If applicable)	7a. NAME OF MONITORING ORGANIZATION Space Systems Division
6c. ADDRESS (City, State, and ZIP Code) El Segundo, CA 90245-4691		7b. ADDRESS (City, State, and ZIP Code) Los Angeles Air Force Base Los Angeles, CA 90009-2960
8a. NAME OF FUNDING/SPONSORING ORGANIZATION	8b. OFFICE SYMBOL (If applicable)	9. PROCUREMENT INSTRUMENT IDENTIFICATION NUMBER F04701-88-C-0089

8c. ADDRESS (City, State, and ZIP Code)	10. SOURCE OF FUNDING NUMBERS			
	PROGRAM ELEMENT NO.	PROJECT NO	TASK NO	WORK UNIT ACCESSION NO.

11. TITLE (Include Security Classification)

Plasma Wave Observations During Ion Gun Experiments

12. PERSONAL AUTHOR(S) Olsen, R. C. and Weddle, L. E. (Naval Postgraduate School) and Roeder, J. L. (The Aerospace Corporation)

13a. TYPE OF REPORT	13b. TIME COVERED FROM _____ TO _____	14. DATE OF REPORT (Year, Month, Day) 1990 March 20	15. PAGE COUNT 42

16. SUPPLEMENTARY NOTATION.

17.	COSATI CODES		18. SUBJECT TERMS (Continue on reverse if necessary and identify by block number)
FIELD	GROUP	SUB-GROUP	Space Environment Satellites

19. ABSTRACT (Continue on reverse if necessary and identify by block number)

Experiments in charge control on the AF/NASA P78-2 (SCATHA) satellite were conducted with a plasma/ion source in the inner magnetosphere. These experiments were monitored with plasma wave instruments capable of high temporal and frequency resolution in the 0 to 6 kHz frequency range. Ion gun experiments revealed two distinct classes of behavior. Non-neutralized ion beam operation at 1 mA, 1 kV resulted in arcing signatures (spiky in time, broad frequency range), coincident with induced satellite potentials of -600 to -900 V. This signature disappeared when the accelerating voltage was switched off or the beam was neutralized (at which time the satellite body approached potentials of a few volts). The signal is attributed to arcing between differentially charged surfaces. An additional feature was noted in the 100 kHz channel of the wave receiver. During emission of dense, low energy plasma, a signal is generated which may be at the upper hybrid, or plasma, frequency for the local plasma.

20. DISTRIBUTION/AVAILABILITY OF ABSTRACT ☒ UNCLASSIFIED/UNLIMITED ☐ SAME AS RPT. ☐ DTIC USERS	21. ABSTRACT SECURITY CLASSIFICATION Unclassified	
22a. NAME OF RESPONSIBLE INDIVIDUAL	22b. TELEPHONE (Include Area Code)	22c. OFFICE SYMBOL

DD FORM 1473, 84 MAR   83 APR edition may be used until exhausted   SECURITY CLASSIFICATION OF THIS PAGE

All other editions are obsolete   UNCLASSIFIED

PREFACE

Accession For

NTIS   GRA&I

DTIC TAB

Unannounced

Justification

A-1

1

CONTENTS

FIGURES

I. INTRODUCTION

A. PROBLEM OF SATELLITE CHARGING

A satellite orbiting in the ionosphere or magnetosphere is essentially a probe in a plasma. It is not surprising, therefore, that a satellite behaves much as a Langmuir probe in a laboratory setting, acquiring a net charge with respect to the ambient plasma. The resulting potential (or potential energy, $q \phi$) is typically comparable to the thermal energy (kT_e) of the plasma. This is not generally a problem at low altitudes, where the thermal energies are low, but at high altitudes it has long been recognized that satellite surfaces can charge many kilovolts negative with respect to the environment, and with each other. Such charging has been associated with satellite anomalies and failures.[1,2]

The commonly accepted mechanism for such anomalies is arcing on the satellite surface between differentially charged insulators, with resulting physical damage, or an electromagnetic pulse into the satellite command/ control systems.[3] This satellite failure mode is motivation for studies of the processes involved in satellite charging and the methods for controlling the charging, particularly active control techniques.

B. HISTORY OF ACTIVE EXPERIMENTS

1. CHARGING EXPERIMENTS

A limited number of active satellite charging experiments have been carried out. Experiments with the Applied Technology Satellites 4,5, and 6 offer most of the available data on active charge control at high altitudes.[4,5] At lower altitudes, experiments with the SERT II payload, designed to test ion engine technology, were conducted at 1000 km altitude with limited instrumentation.[6,7] Rocket experiments, such as the Porcupine ion beam experiment, have provided brief glimpses of the behavior of such systems[8,9]. More recently, results from the ARCS experiments have become available.[10]

2. PLASMA WAVE OBSERVATIONS

ATS satellites, which provide the bulk of our knowledge on the results of active charge control experiments, did not carry plasma wave receivers, so our information is limited in that respect. Information on the effects of ion beam emission is particularly limited. The main experiments in this domain are the Porcupine and ARCS rocket experiments.[8,9,10,11] The Porcupine experiment used a 200 eV Xe^+ ion gun, which resulted in production of ion cyclotron, and more generally, lower hybrid waves in the oxygen-dominated topside ionosphere.[12,13,14]

Higher frequency phenomena were reported for the Porcupine experiments by Pottelette et al.[15] and Thiel et al.[16] High frequency (e.g., MHz) turbulence was observed. The data were interpreted as the result of coupling between Langmuir plasma waves and a lower hybrid drift instability near the beam source. A separate phenomenon, which was identified at large distances, appeared to result from a density minimum in front of the beam, which destabilized electron cyclotron harmonic waves.[15]

The ARCS rockets carried Ar^+ ion guns. These experiments resulted in observations of numerous low frequency electrostatic emissions, particularly near the lower hybrid frequency.[17,18] The first ARCS experiment was launched on 26 January 1980. The argon beam operated at 100 mA, 25 eV.[11]

The Ar^+ ion generators were flown again on 10 February 1985 on a sounding rocket launched from Sondre Stromfjord, Greenland, to study ion beam dynamics and ion beam effects on the ionosphere. The generators were arranged such that one emitted its beam parallel to the magnetic field, the other perpendicular to the field. During parallel beam operations, emissions were observed near multiples of the H^+ cyclotron frequency and the lower hybrid frequency. Perpendicular beam operations produced emissions at He^+ and O^+ cyclotron harmonics.[19]

The noise generated by the discharge itself is of some pertinence. Signals with wavelengths comparable to the size of the discharge chamber will be stimulated. Kudo et al.[20] report observations of discharge noise characteristics in the laboratory for a 5 cm thruster (apparently using

Mercury ions). They indicate a variety of coherent peaks, depending on operating mode, at least some of which are interpreted as two-stream, instability-generated, ion-acoustic waves.

There have been limited reports on the ion and electron gun experiments conducted on the SCATHA satellite.[21] It was found that electrical discharges and arc-generated pulses could be observed during high voltage electron gun experiments (e.g., 1.5 kV, 6 mA). Similar arcing signatures were observed during nonneutral ion beam experiments. The purpose of this report is to extend this earlier work, based on a survey of the complete data set.[22]

C.   THEORETICAL EXPECTATIONS

A limited number of theoretical calculations have been done for such ion beam experiments. They predict that the hydrogen cyclotron harmonics and the upper and lower hybrid frequencies should be observed.[13,17,18,23,24]

Earlier experiments which were the topic of these theoretical treatments took place in the ionosphere where H^+ is a minor constituent. At geosynchronous orbit the environment is mostly H^+, with O^+ ranging from 10 to 50 percent, and the beam density is large compared to the ambient. The magnetic energy density relative to the plasma energy density (β) is also different in the two regions. While these differences prevent us from applying the results of these calculations to our situation, they do give us ideas on where to start looking. We believe it is reasonable to assume that plasma waves at some frequency would be generated by the SCATHA ion gun. At the SCATHA orbital altitudes, the H^+ cyclotron frequency and the lower hybrid frequency are too low to be observed by the SC1 experiment, although a second receiver (SC10) is occasionally available for this lower frequency regime. The electron cyclotron frequency was generally a few kilohertz. The majority of the work which follows deals with this higher frequency range. Unfortunately, the plasma frequency and upper hybrid resonance frequency are not generally within the wideband receiver frequency range.
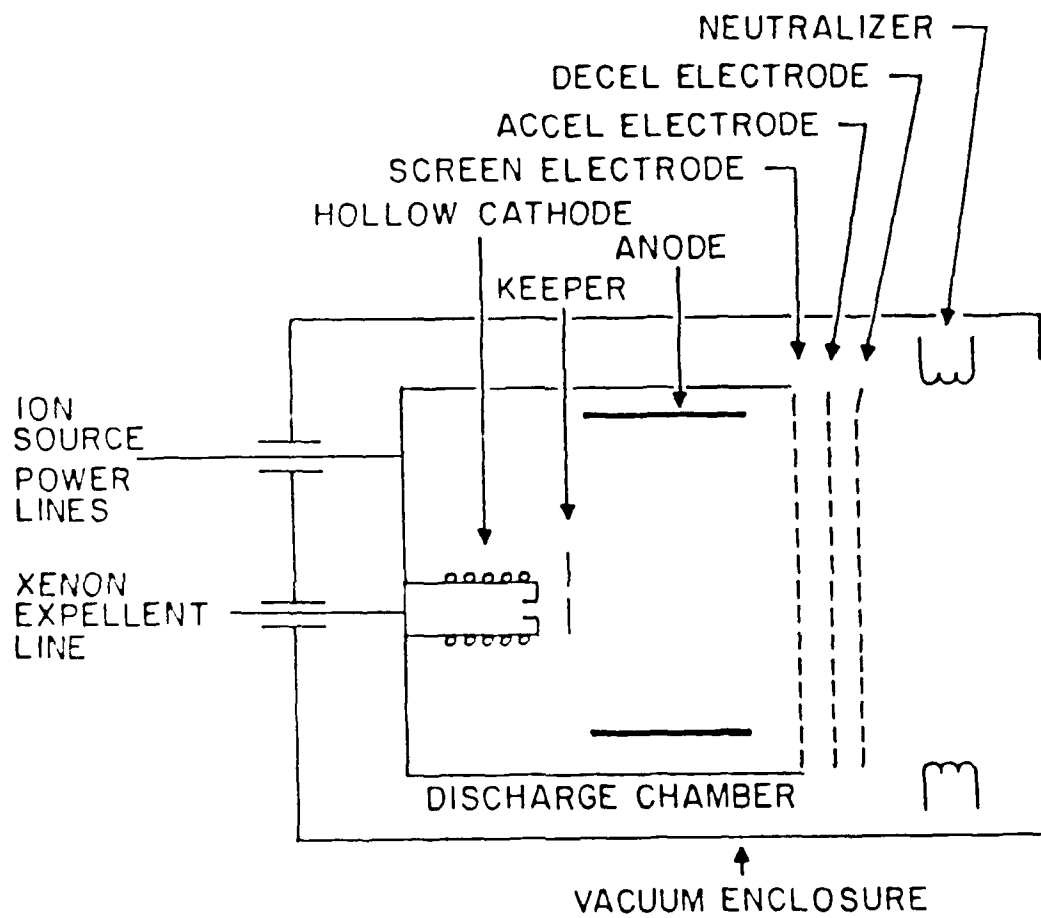
D.   THE SCATHA PROGRAM

1.   P78-2 SATELLITE

The Air Force P78-2 satellite was launched on 30 January 1979, as part of the joint NASA/Air Force program on Spacecraft Charging at High Altitudes (SCATHA).[25] The satellite was placed in a near geosynchronous orbit, at 7.9° inclination, 5.3 RE perigee, and 7.8 RE apogee. The satellite was spin stabilized, with a rotational period of about 59 seconds. The spin axis was oriented perpendicular to the earth-sun line, roughly in the orbital plane. Hence, at local midnight, the spin axis was pointing east. The cylindrically shaped satellite measured roughly 1.7 m in diameter and 1.75 m in length. The surface was made up of both insulated and conducting materials. The sides were primarily insulating solar cell glass covers. The satellite was instrumented with an abundance of instruments designed to observe charging effects.[22,25] In addition, it carried two active charge control experiments and a plasma wave receiver.

2.   XENON ION GUN

An ion source, designated SC4-2, was provided to emit neutralized and nonneutral beams at energies of 1 and 2 kV, at nominal currents of 0.3, 1.0, and 2.0 mA. Xenon propellant was utilized in the hollow cathode based system by Masek and Cohen.[26] The beam neutralization was provided by filament neutralizers, which could be biased in voltage and set at fixed current levels. Since the filament current was not allowed to float, there was generally a small imbalance in the emitted currents, in the beam neutralized mode. This resulted in nonzero satellite potentials observed during such operations. A few essential features of the source are further illustrated in Figure 1. The hollow cathode source inside the chamber had a separate "keeper" anode, which was generally used to start the discharge inside the chamber. The main discharge then was struck to the anode rings along the walls of the discharge chamber. The plasma was extracted by applying high voltage to the grids. With no voltage applied to the grids, but full power to

10

NEUTRALIZER —

DECEL ELECTRODE —

ACCEL ELECTRODE —

SCREEN ELECTRODE —

HOLLOW CATHODE

ANODE

KEEPER

ION
SOURCE
POWER
LINES

XENON
EXPELLENT
LINE

DISCHARGE CHAMBER

VACUUM ENCLOSURE

SC4 - 2 ION GUN

Figure 1. Ion Gun Block Diagram

11

the discharge, a low current, low energy plasma could be emitted. This mode was termed "trickle" mode. The charging results from SC-4 experiments have been studied by Werner.[27]

D.3 DETECTORS - SC-1/SC-10

The plasma wave receiver (SC1-8) had two operational elements of interest. It could be connected to the long electric antennas (SC-10), which were 100 m tip-to-tip, or to the air-core magnetic loop antenna. The magnetic loop is on a 2 m boom, with an effective area of 575 m^2 at 1.3 kHz. The magnetic receiver has a sensitivity of 3×10^{-6} $nT/Hz^{1/2}$ at 1.3 kHz, and a 60 dB dynamic range. Each of the electric antennas are insulated for the first 30 m of length, then exposed for the remaining 20 m. The electric field receiver has a sensitivity of 5×10^{-7} V/m $Hz^{1/2}$ and a set of 8 filter channels with bandwidth ±7.5% at frequencies of 0.4, 1.3, 2.3, 3.0, 10.5, 30, 100, and 300 kHz. Only the filter data are routinely available. Experiments described below were selected for the availability of wideband data. A lower frequency wideband channel (0 to 400 Hz) is available from the SC-10 and SC-11 (magnetometer) experiments when SC1-8 is in the 0 to 3 kHz mode. Unfortunately, the 0 to 400 Hz wideband data were not originally considered, and the tapes were unreadable when we attempted to reprocess the data for the low frequency wideband range. Four lower frequency channels are filtered from the SC-10 and SC-11 measurements at 0.1 to 1.0, 1.0 to 2.0, 2.0 to 20.0, and 20.0 to 200.0 Hz.

II. OBSERVATIONS

A. INTRODUCTION

Early analysis of the plasma wave data during ion gun operations generally showed signatures which were consistent with pulses generated by arcing.[21] There was some ambiguity in the data as to whether the arcing was internal to the ion gun or external. Considerations presented below have indicated that the arcing is occurring on the satellite skin, that is, between differentially charged insulating surfaces or between the insulators and the satellite body.

Three ion gun modes were studied. First, the primary mode for satellite charge control is with both the ion beam and neutralizer on. The satellite is thus emitting a neutralized ion beam. Next, induced (negative) charging experiments were conducted with the ion beam on and the neutralizer off. Only xenon ions are emitted in this mode. Finally, in trickle mode the ion beam discharge is on, but without an accelerating voltage on the grids. Data taken in each of these three modes will be presented.

B. DAY 200, 2214-2314 UT

The first plasma wave observations presented here are from a sequence of ion gun experiments on 19 July 1979 (Day 200). These data illustrate typical observations for:

1. gun off

2. gun and high voltage on, neutralizer off

3. gun on, high voltage and neutralizer off (trickle mode)

The satellite location is near local dusk (1954-2042 LT), between $L = 7.6$ and 8.0. The electron cyclotron frequency varies from 1.8 to 2.2 kHz. The hydrogen cyclotron frequency is around 1 Hz, and the lower hybrid frequency is about 40 to 50 Hz--hence these latter two fundamental frequencies are off scale.

13

The plasma wave (wideband) data set presented below began while the ion gun was on with an accelerating voltage of 1 kV and a nominal beam current of 2.0 mA. The neutralizer filament power was off. The satellite was in the dusk bulge region, in a relatively quiet plasma sheet environment. The mainframe was uncharged (<±10 V) when the gun was off, and charged to approximately -800 V when the gun was on, in the nonneutralized mode.

The operation is summarized in Figure 2, where the narrowband filter data for the period 2130-2330 UT are presented for both antennas. The ion gun experiments begin at 2130 (system power on) and end at 2300 UT. The 20 to 30 dB increases in (electric) amplitude at 400 Hz, 1.3 kHz, 2.3 kHz, and 3.0 kHz correspond to operation of the nonneutralized ion beam. Drops in amplitude at 2200 and 2230 occur at times when the accelerating voltage is switched off, sending the gun into trickle mode. Charging analysis shows that the 1 kV beam charged the satellite to potentials of -600 to -800 V when the high voltage was on. Trickle mode results in near-zero voltages.[27]

The data presented in Figure 2 are heavily processed and smoothed. Figure 3 shows the raw data for the 400 Hz and 100 kHz channels, with the electric antenna in the top two panels. The substantial fluctuations in the data are typical of the other channels.

The magnetic field data (Figure 2) show that at 400 Hz the amplitude increase is greater than 40 dB and that the signal peaks off the scale (at ~ 15 dB). The 1.3 to 3.0 kHz channels show magnetic field amplitude increases of 35 to 40 dB. During trickle mode the magnetic field amplitudes show a decrease, but remain 15 to 30 dB above background. We interpret the trickle mode data as showing that no interference generated at these lower frequencies reaches the electric antenna, but that an electrostatic or electromagnetic signal is caused by the interaction of the "dense" xenon plasma from the gun with the ambient plasma in the immediate vicinity (a few meters) of the satellite, and this signal is observed by the magnetic loop antenna. In contrast to the low frequency observations, the 100 kHz electric field channel (Figure 3) shows an increase in signal strength during trickle mode. Note that the fluctuations in the 100 kHz signal are minimal during trickle mode compared to the HV-on data.
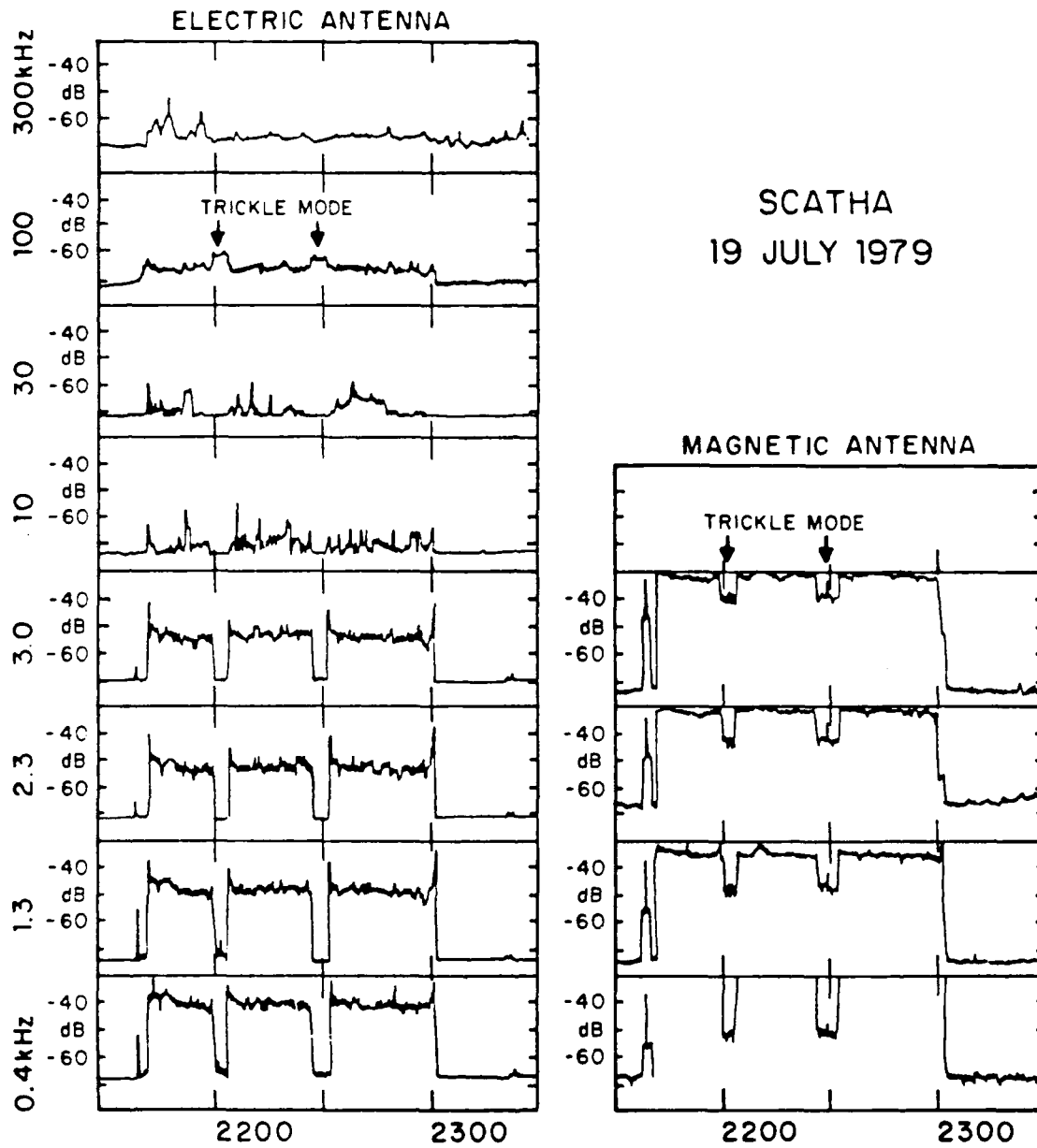
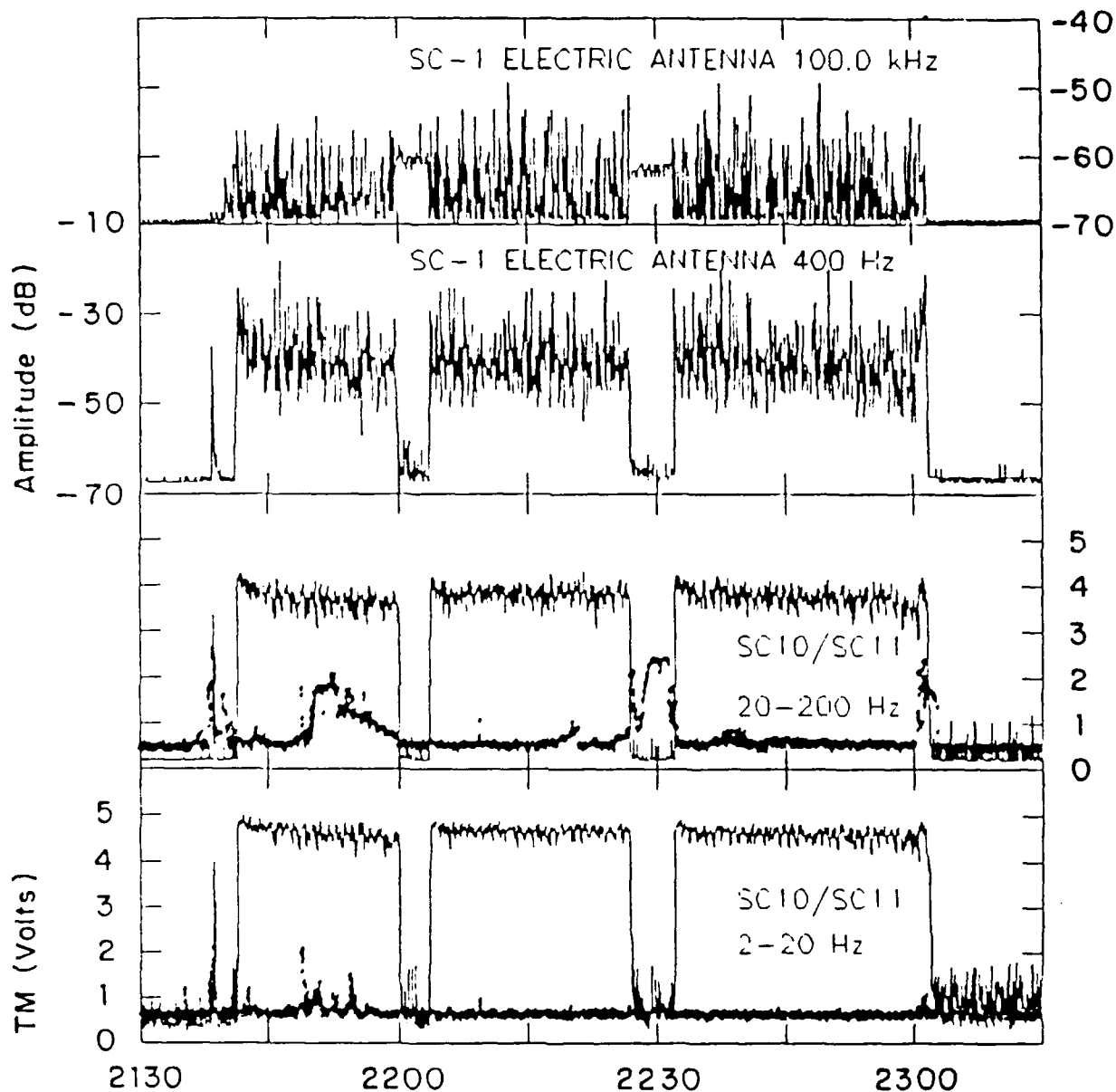Figure 2. Plasma Wave Intensities, Day 200

15

Figure 3. Detailed Plot of SC1 and SC10/11 Plasma Wave Data. The top two panels show the 100 kHz and 400 Hz electric antenna data. The bottom two panels show the SC10/11 data. The electric field (SC10) data are plotted as a thin line. The magnetometer (SC11) data are plotted as dots, and generally lie below the SC10 data.

Two of the lower frequency filtered outputs from the quasi-static electric field and magnetometer experiments are presented in the lower half of Figure 3. The vertical axis is telemetered voltage, which has a peak of 5.1 V. The electric field data (thin, solid line) in the three lowest channels are all similar to the 2 to 20 Hz data (bottom panel). The receiver nearly saturates with the gun on. The magnetometer data from the axis parallel to the spin axis (solid dots) do not show any correlation with the gun operations in the three lowest frequency channels. The 20 to 200 Hz magnetic channel shows a substantial response during trickle mode (2230 UT) and again at gun off (~ 2300 UT). The response at ~ 2300 UT corresponds to a decrease in the beam current setting to 0.3 mA, just prior to turning the gun off. The difference in magnetometer (SC-11, 20 to 200 Hz) and search coil (SCI-8, 400 Hz) behavior suggests that the search coil response is due to the electrostatic coupling of the search coil to the electric field emissions. The magnetometer is not susceptible to this type of artifact. The search coil data are therefore interpreted as the near-field (2 m from spacecraft) electrostatic measurements, to be contrasted with the far-field data from the long electric antenna (25 m average).

The details of the plasma wave observations are addressed by means of the wideband data. The wideband data are presented in spectrogram and line plot formats. Typical "gun-off" data are shown in line plot form in Figure 4. The 19 July 1979 broadband data were taken with the plasma wave receiver in the 0 to 3 kHz mode.

Figure 4A shows a frequency spectrum of the magnetic field taken at 2302:59 UT with the gun off. Three-second averages were used to create the frequency spectra presented here. There are monochromatic signals at 700 Hz and 2100 Hz, along with a broad background spectrum peaked at 1 kHz. These monochromatic signals are caused by a 700 Hz tuning-fork driver circuit in another experiment and are not seen in the electric field data. The broad peak is the resonant response of the receiver to a white noise input, as determined by ground calibration. This noise is not visible in the electric field (E) data. Figure 4B shows the frequency spectrum for the electric field data taken at 2303:05 UT with the gun off. Two peaks are found at 2570 and
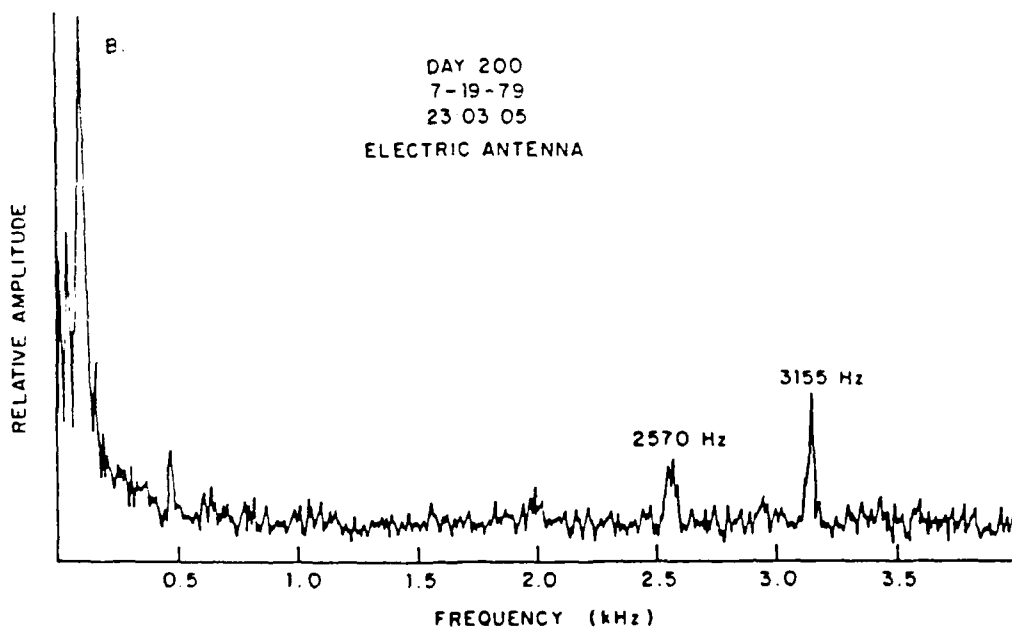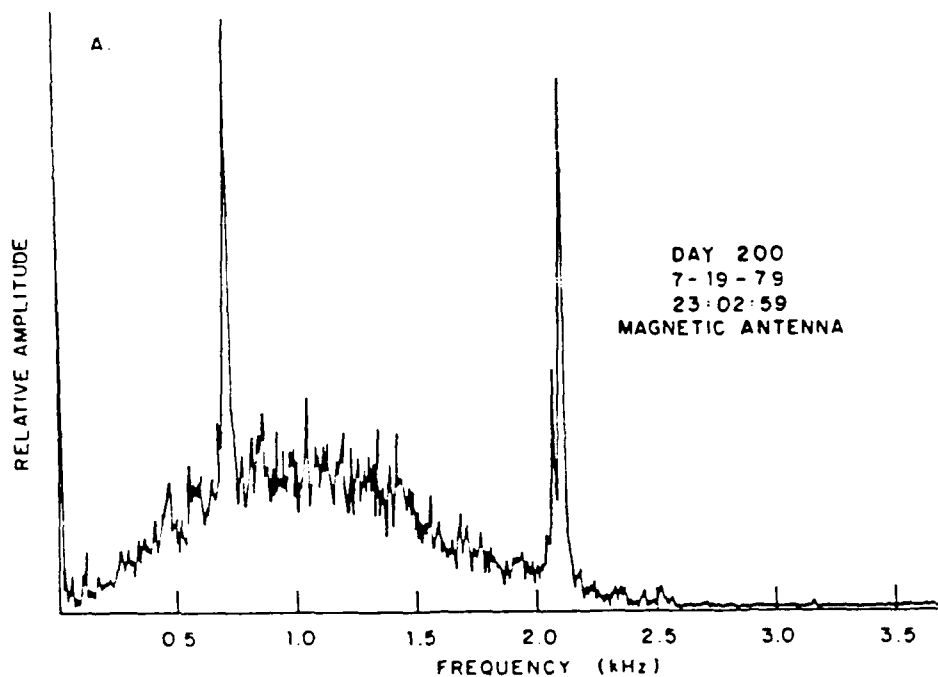
17

Figure 4. A) Magnetic Loop Antenna Spectrum, Gun off, 2303:05 UT
B) Electric Antenna Spectrum, Gun off, 2303:05 UT

18

3155 Hz. At least one of the signals is probably the electron cylotron harmonic, or $(3/2)f_{ce}$.[3] The low frequency peak (about 100 Hz) may be an artifact generated on or near the spacecraft. A substantial study of this phenomenon by Koons and Holzworth (private communications) was unable to resolve this point. If natural, it is a previously unreported feature of magnetospheric plasma wave morphology. It is near the low frequency cutoff of the receiver band-pass.[21]

The nonneutralized, 1 kV, 2.0 mA beam experiment is presented next. Data are shown at 2218 UT, in the middle of the second induced charging sequence. The satellite potential is ~ -800 V. Figure 5A is a spectrogram showing 46 seconds of plasma wave for this ion gun operating mode. The horizontal axis is time in seconds, the vertical axis is frequency. All the spectrograms shown here utilize a 0 Hz to 4.0 kHz frequency scale. Signal strength is indicated using a grey scale, with white for low amplitude, black for high. The bandwidth in this mode introduces a roll-off at 3 kHz, as seen in the spectrogram. The plasma wave receiver on the satellite switches antennas every 16 seconds, cycling between the electric field antenna and the magnetic field antenna. Hence, the spectrograms cycle between the electric field data and the magnetic field data every 16 seconds. This spectrogram shows the receiver background noise normally present in the magnetic field (B) data. Again, the selected antenna was switched every 16 seconds, and the roll-off at 3 kHz is due to the receiver mode. There is a broad maximum from 1.0 to 1.5 kHz visible in the magnetic field data as shown by the darkening of the spectrogram at those frequencies. This signal is not present in the electric field data. Brief, vertical striations in the data, particularly the magnetic data, show a broad spectrum which we interpret as the signal generated by arcing on or in the satellite. The vertical striations are obviously due to pulses with periods considerably less than a second. Indeed, since the frequency spectrum extends to kHz, the duration of the pulses is of the order of milliseconds or less.

The frequency spectrum is analyzed in more detail in the following two figures. Figure 6A is a frequency spectrum of the magnetic field data at 2218 UT. The spiky aspects attributed to arcing have largely been averaged

SCATHA
19 July 1979

A.

B.
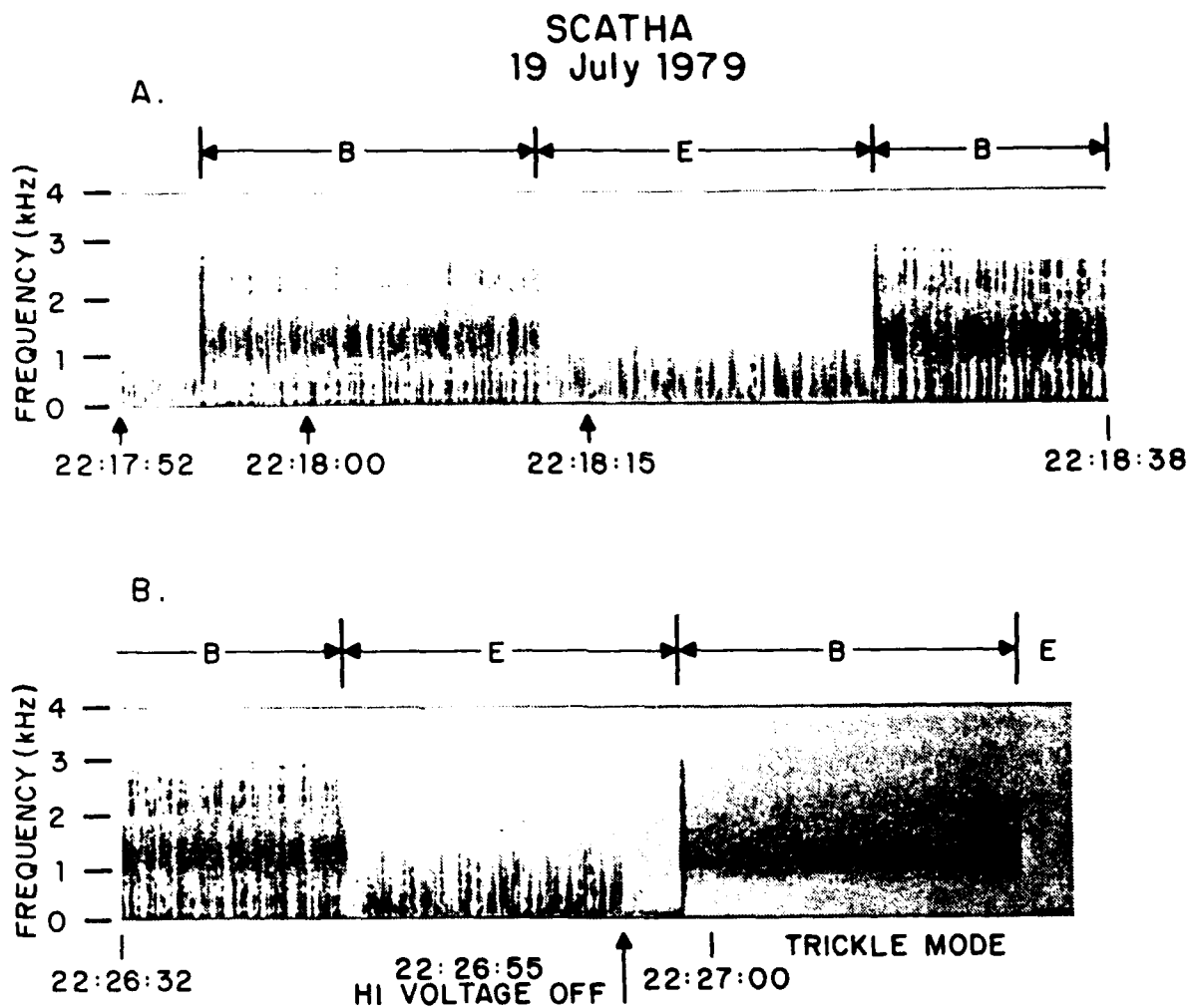
Figure 5.   A) Plasma Wave Spectrogram for Day 200.   Gun on, HV on,
1 kV, gun current = 2 mA.   Neutralizer is off.
B) HV off at 22:26:55; Ion Gun Goes into Trickle Mode.

20

A.

DAY 200
7-19-79
22 18 00
MAGNETIC ANTENNA

RELATIVE AMPLITUDE

0.5   1.0   1.5   2.0   2.5   3.0   3.5

FREQUENCY (kHz)

B.

DAY 200
7-19-79
22 18 15
ELECTRIC ANTENNA

RELATIVE AMPLITUDE

~ 3.1kHz

0.5   1.0   1.5   2.0   2.5   3.0   3.5

FREQUENCY (kHz)

Figure 6.   A) Magnetic Loop Antenna Spectrum, Gun on, HV on (1 kV)
            B) Electric Antenna Spectrum, Gun on

out by three-second averaging. Figure 6A shows that the most intense average signals are below 500 Hz, followed by a broad peak from 1.1 to 1.4 kHz. This latter peak is the broad maximum visible in the spectrogram and is similar to the receiver noise signal shown in Figure 4A. Consideration of calibrated filter data (Figure 2) show that this signal is orders of magnitude higher in amplitude than background noise. This appears to be, therefore, the system response to an intense white noise input signal. Figure 6B shows the frequency spectrum of the electric field data at 2218:15. A broad signal, from near zero to about 1.5 kHz and monotonically decreasing in amplitude, is found in Figure 6B that was not present in the gun-off data of Figure 4B. The smaller peaks near 2.5 and 3.1 kHz are still visible. Hence, the ambient signal persists, or a similar resonance is being driven. The low frequency spectrum is similar to that found in the magnetic field data of Figure 6A, but there is not a corresponding signal in the 1.0 to 1.4 kHz range of the electric field spectrum. The small peak at 3.1 kHz is again thought to be the $(3/2)f_{ce}$ signal (f_{ce} = 2.1 kHz at this time).

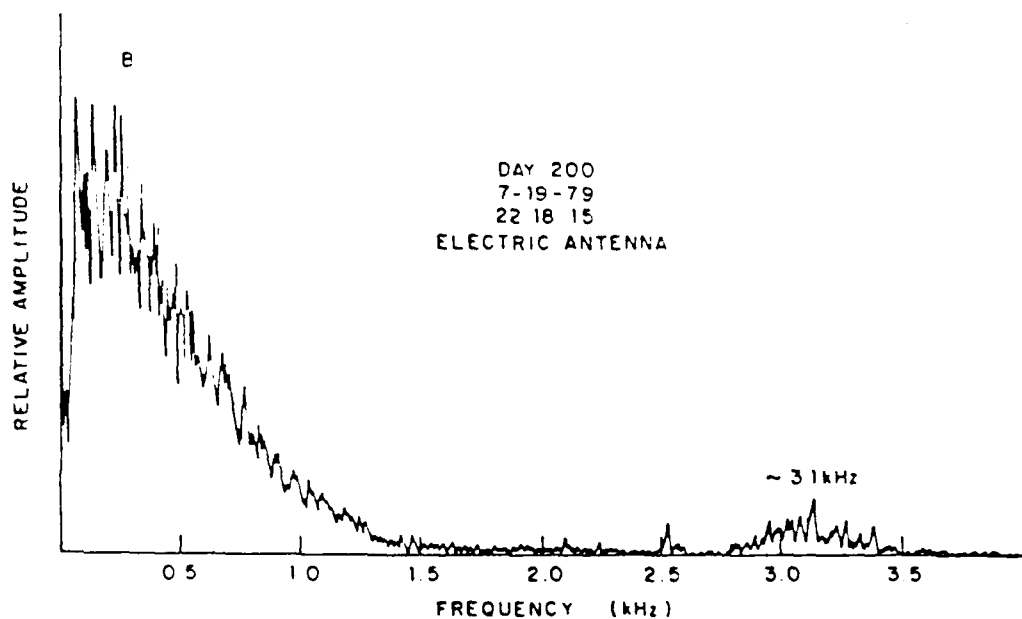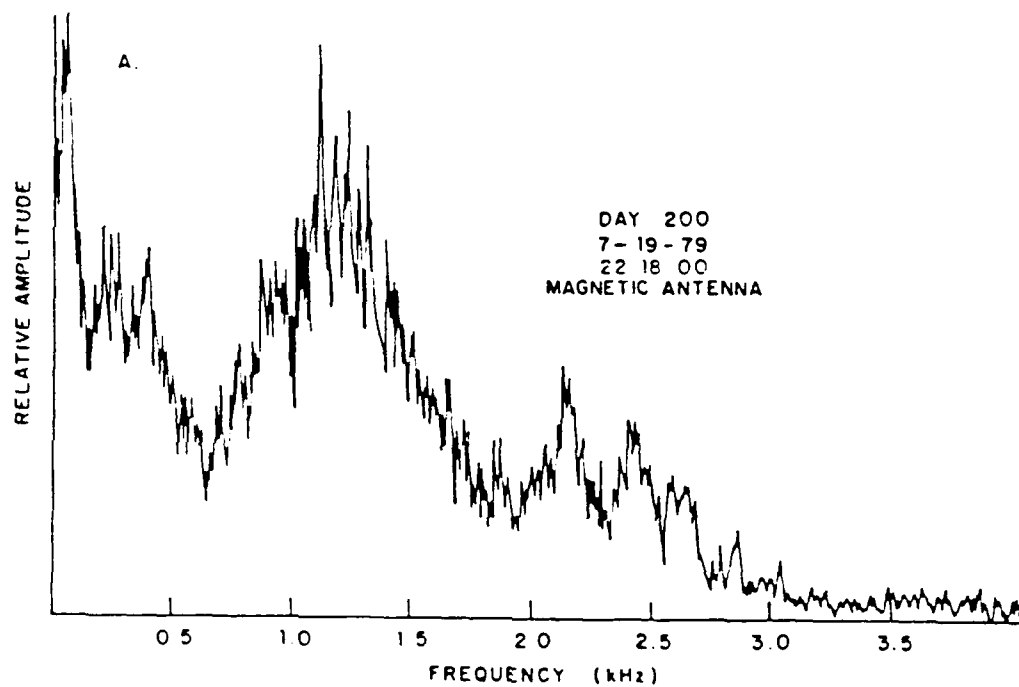At 2226:55 the high voltage is turned off, resulting in trickle mode. A net ion current of 20 to 50 µA is still being emitted (according to gun diagnostics). The result of this ion emission is a satellite potential near zero (<±10 V). The arcing response seen in Figure 5A ceases during an electric field measurement, as shown by Figure 5B. As previously noted (Figure 3), the electric narrowband channels from 0.1 Hz to 3.0 kHz drop to background, but there is an enhancement at 100 kHz. The 400 Hz to 3.0 kHz magnetic field channels show a decrease, but the signals are well above the gun-off values.

Figure 5B shows that the broad maximum from 1.0 to 1.5 kHz is still present during trickle mode in the magnetic data, while the electric field spectrum no longer shows the 0 to 1 kHz signal. The signals become cleaner over the next few minutes. By 2229 both the broadband signal in the magnetic field data and the very low frequency signal in the electric field data have become more intense, but have not substantially changed in character. The 3.2 kHz signal in the electric field data persists. Figure 7 is a frequency spectrum for the magnetic field data at 2229:45. The broad peak from 1.0 to

DAY 200
7 - 19 - 79
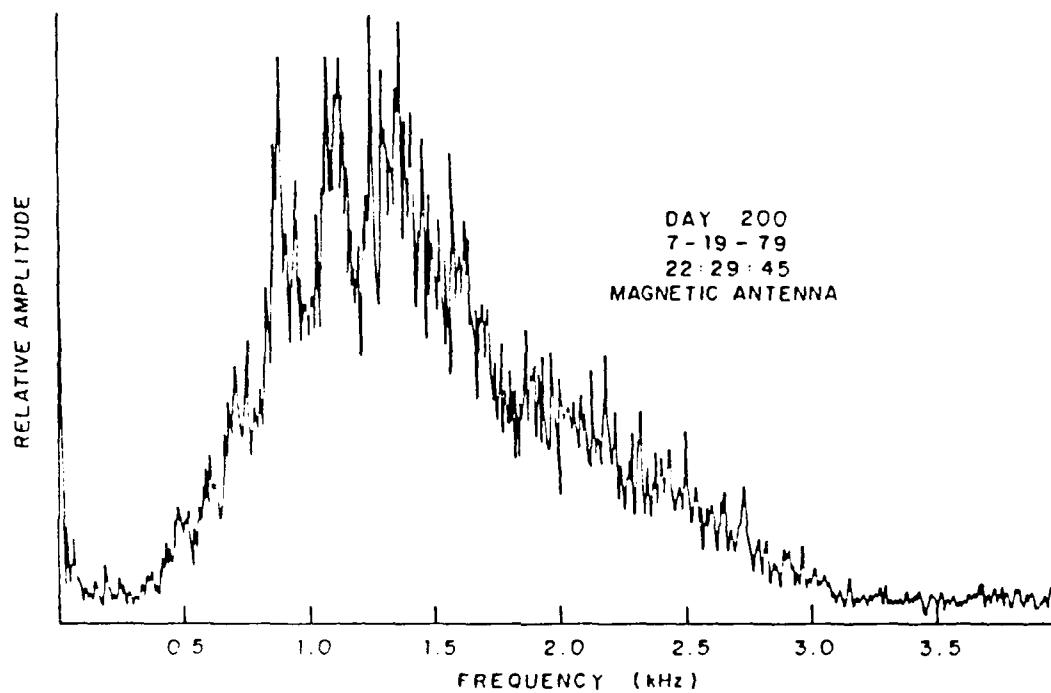22:29:45
MAGNETIC ANTENNA

Figure 7. Magnetic Antenna Spectrum, Day 200, HV Off (Trickle Mode)

1.5 kHz is similar to that found previously, that is, similar to the receiver resonance response to a white noise input. The lower frequency peak (below 500 Hz) seen in Figure 6A is now gone.

At 2232:03 (not shown) the high voltage is turned back on. The arcing resumes, and the data resume their former character. The signals do appear more intense in the spectrogram, but this is probably an artifact of AGC and processing variations. This change in the data could reflect different characteristics of differential charging following the trickle-mode induced discharge of the dielectric materials.[5,27]

There are changes in the data which are independent of gun status change. One to two minutes after each trickle mode operation, the amplitude of the waves seen with high voltage on drop by 5 to 10 dB, as visible in Figure 2, for the electric channels. The spectrum is largely unchanged, however.

Changes in the gun current resulted in changes in the wave data. Figures 8 and 9 show the results of decreasing the gun current, just prior to the end of the gun experiments on this day. Figure 8A shows the wideband data while the gun is in its 2 mA mode (nominal current is 1.7 mA at this time). The main features, seen previously, are the broadband signal peaking near 1 kHz in the magnetic channel, a lower frequency broadband signal in the electric channel, and numerous vertical striations which appear to indicate arcing. The beam current is reduced to 1.0 mA at 2258:06, during a "B" sample period. There are no immediately obvious effects in the spectrogram, nor in the narrowband data (Figure 9). Within the next minute, however, it becomes apparent that the frequency of occurrence of the striations has decreased. This is illustrated in Figure 8B, and is most obvious in the magnetic data at 2300:10. The beam current is further reduced at 2300:22 to 0.3 mA during an "E" sample period (Figure 8C). The immediate results are not obvious, but the subsequent B sample clearly indicates substantially fewer striations. Fifty seconds later (2301:10), the magnetic data are almost free of the arcing signature (Figure 8D), as are the subsequent electric antenna data. The gun is switched off at 23:10:40, during a "B" sample, and the broadband data drop to background.
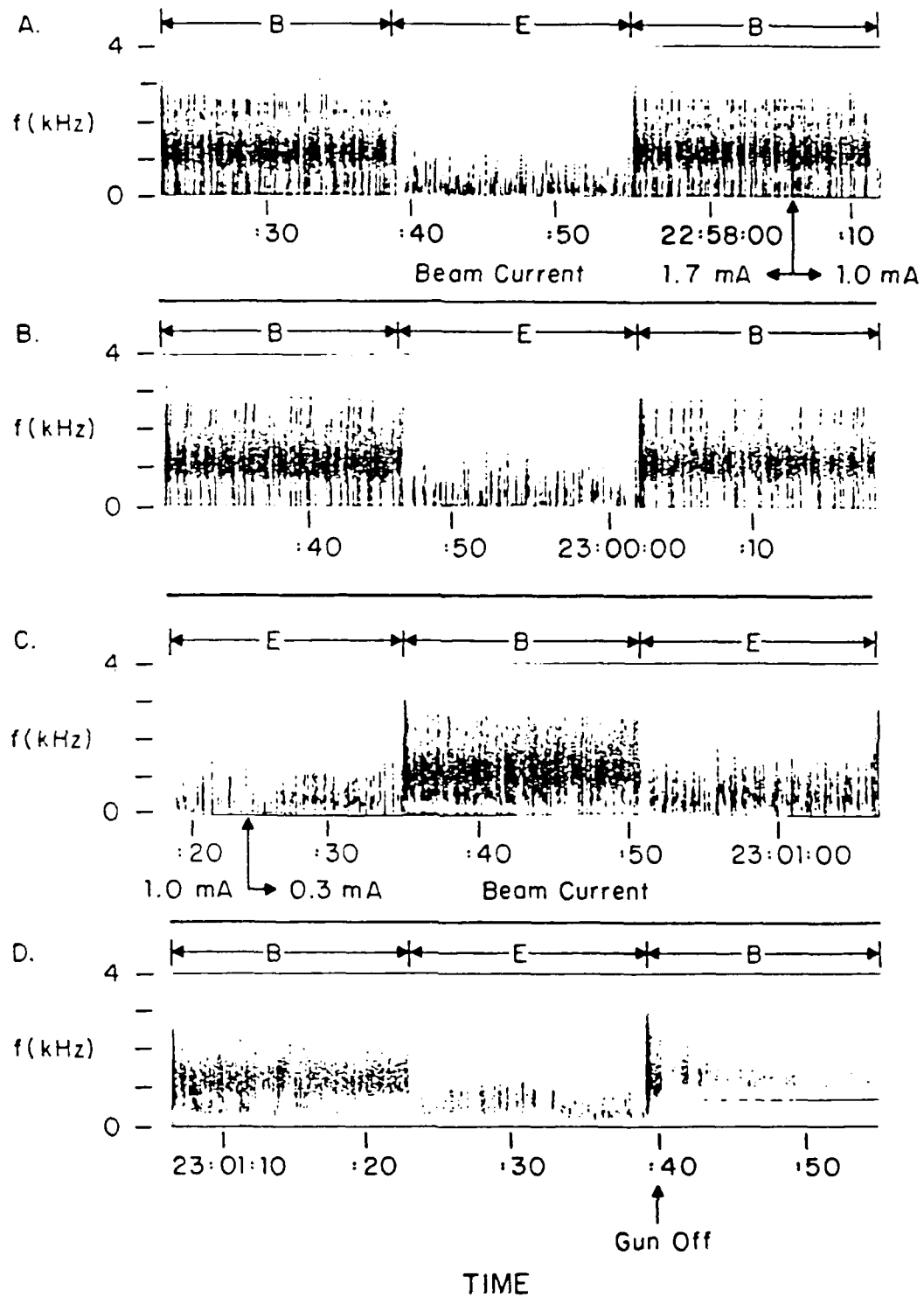
SCATHA
19 JULY 1979

Figure 8. Plasma Wave Spectrograms for Day 200. Segments B, C, and D are sequential in time
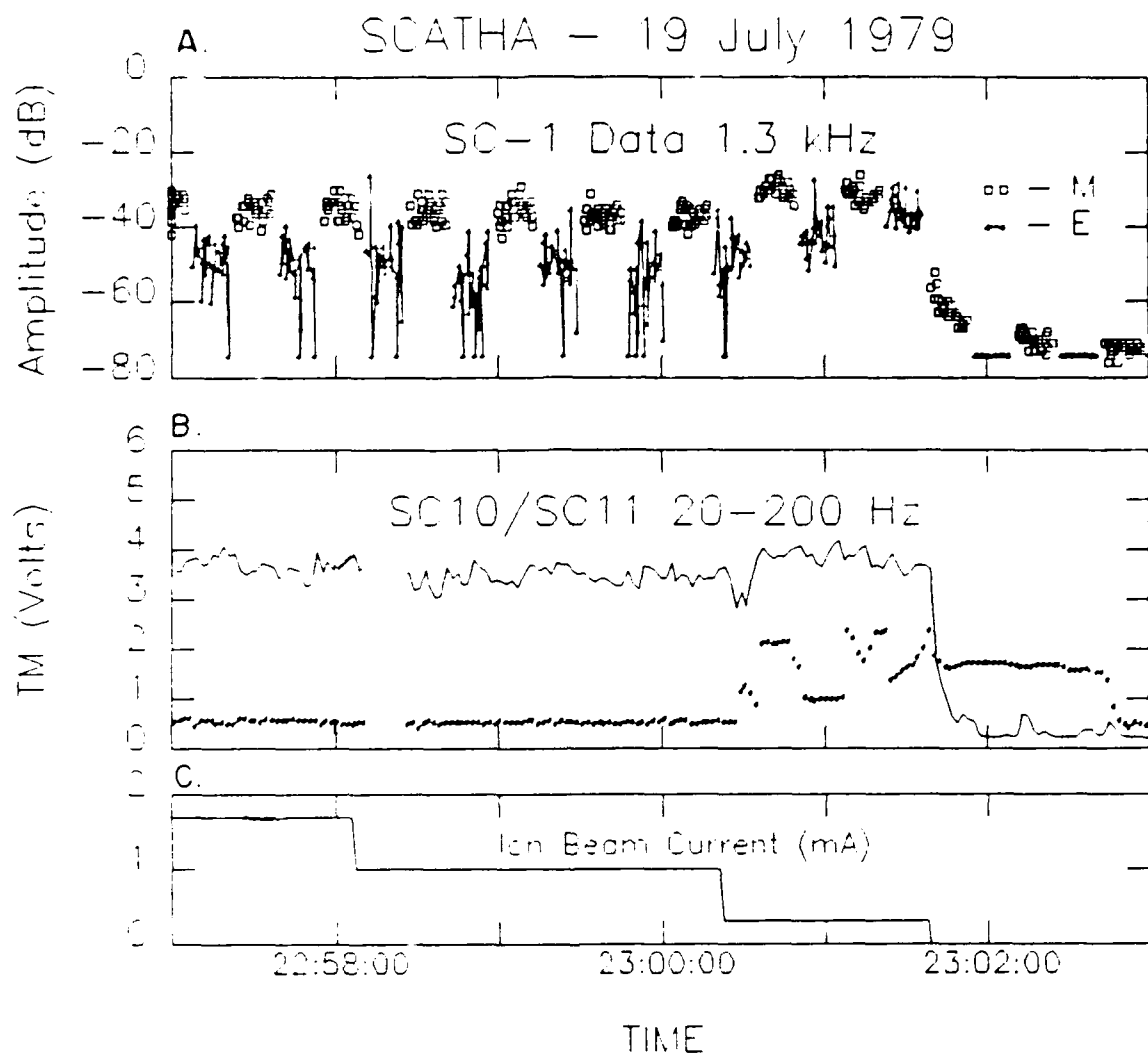
25

Figure 9. Plasma Wave Data for Day 200 as the Gun Current is Reduced to Zero

The narrowband data at 1.3 kHz are shown in Figure 9, along with the 20 to 200 Hz channel of the SC-10 and SC-11 instruments. The 1.3 kHz channel is typical of the 4 lower frequency SC1 channels during this time segment, and was chosen as corresponding to the apparent peak of the magnetic wideband channel. The SC10/SC11 plot is simply an expansion of the latter portion of Figure 3. These data indicate that there is little change in the signals in either receiver when the current is dropped to 1.0 mA (bottom panel). A substantial change is found at 0.3 mA. The 1.3 kHz magnetic antenna amplitude increases by about 10 dB; the electric antenna amplitude increases by some 20 dB. The increase in the SC10 (electric) antenna response is modest, but noticeable. The magnetometer response (SC11) is substantial, as previously noted in the discussion of Figure 3.

Note that these changes do not arise from a cessation of satellite charging. Since the beam current is ~ 1 order of magnitude greater than necessary to induce a kilovolt potential, beam limiting mechanisms are at work. One mechanism which would give this effect is the buildup of space charge outside the gun aperture, causing the beam to stall. Only a few percent of the emitted ions escape. The 0.3 mA beam produces a lower ion density (for constant voltage, or ion velocity). The result in general is a more negative satellite potential, indicating more ions escape. Indeed, the satellite potential apparently drops from about -800 V at 1.7 mA beam current, to -900 V to -1 kV at 0.3 mA beam current.[27]

C.   2 APRIL 1979, 1513-1548 UT

The second operation to be presented occurs in eclipse on Day 92 of 1979. Plasma wave response to gun operations appear similar to those observed in the dusk bulge region on Day 200. This example extends those shown previously by including the effect of beam neutralization. Beam neutralization prevents substantial induced satellite charging by the ion beam, and hence, arcing on the surface. During this period, the satellite is between L=7.3 and 7.6, just after local midnight. The satellite is in eclipse from 1430:00 to 1537:53. The electron cyclotron frequency varies from 3.2 to 3.6 kHz, the hydrogen cyclotron frequency is about 2 Hz, and the lower hybrid frequency

27

varies from 75 to 85 Hz. Only the spectrograms (Figure 10) and narrowband data (Figure 11) for this period are shown. Attempts to generate amplitude plots for the frequency spectrum were not successful because of the age of the magnetic tape on which the data are stored. The data for this period were taken in the 0 to 5 kHz receiver mode but are shown only from 0 to 4 kHz. There is no receiver roll-off at 3 kHz in these data.

The data presented next begin with the ion beam on, with beam voltage at 1 kV. The beam current and neutralizer current were set at 1 mA (nominal), with the neutralizer biased -10 V with respect to the ion gun. Net current measurements from the gun indicate a net current of about 100 µA. Charged-particle data are confused during this period, partly due to rapid and frequent ion gun mode changes. Indications are that, on this day, the neutralized beam resulted in potentials of -100 to -200 V, depending on the neutralizer setting. Figure 10A shows that this is a diffuse spectrum in both the electric and magnetic field data. In the magnetic channel there is con- tinuous band of signals from just below 1 kHz to the top of the spectrogram at 4 kHz, with the 1 to 2 kHz region showing slightly greater signal strength. The 700 and 2100 Hz interference lines are not visible. A faint spectrum exists in the electric field data from 0.4 to 1.5 kHz. This diffuse spectrum is regularly seen during such neutralized beam operations. Examination of filter data (presented below) show that this signal amplitude has increased relative to the trickle mode data.

Figure 10A shows how the data change with the neutralizer off (neutral- izer off at 1517:47). The neutralizer-off data resemble the data from Day 200 at similar gun settings. The broad frequency spikes and the intense 1.0 to 1.5 kHz band are both present in the magnetic field data. The electric field data appear similar to the arcing data shown for Day 200. Figure 10B shows data taken as the high voltage is turned off at 1518:50. The gun enters trickle mode at that point. The emitted current is 10 to 50 µA . Visible at this time in the magnetic field data are the 700, 1400, and 2100 Hz interfer- ence lines and the diffuse background noise. The electric field data contains a very low frequency (less than 100 Hz) signal and some spotty signals near 1 kHz.

SCATHA
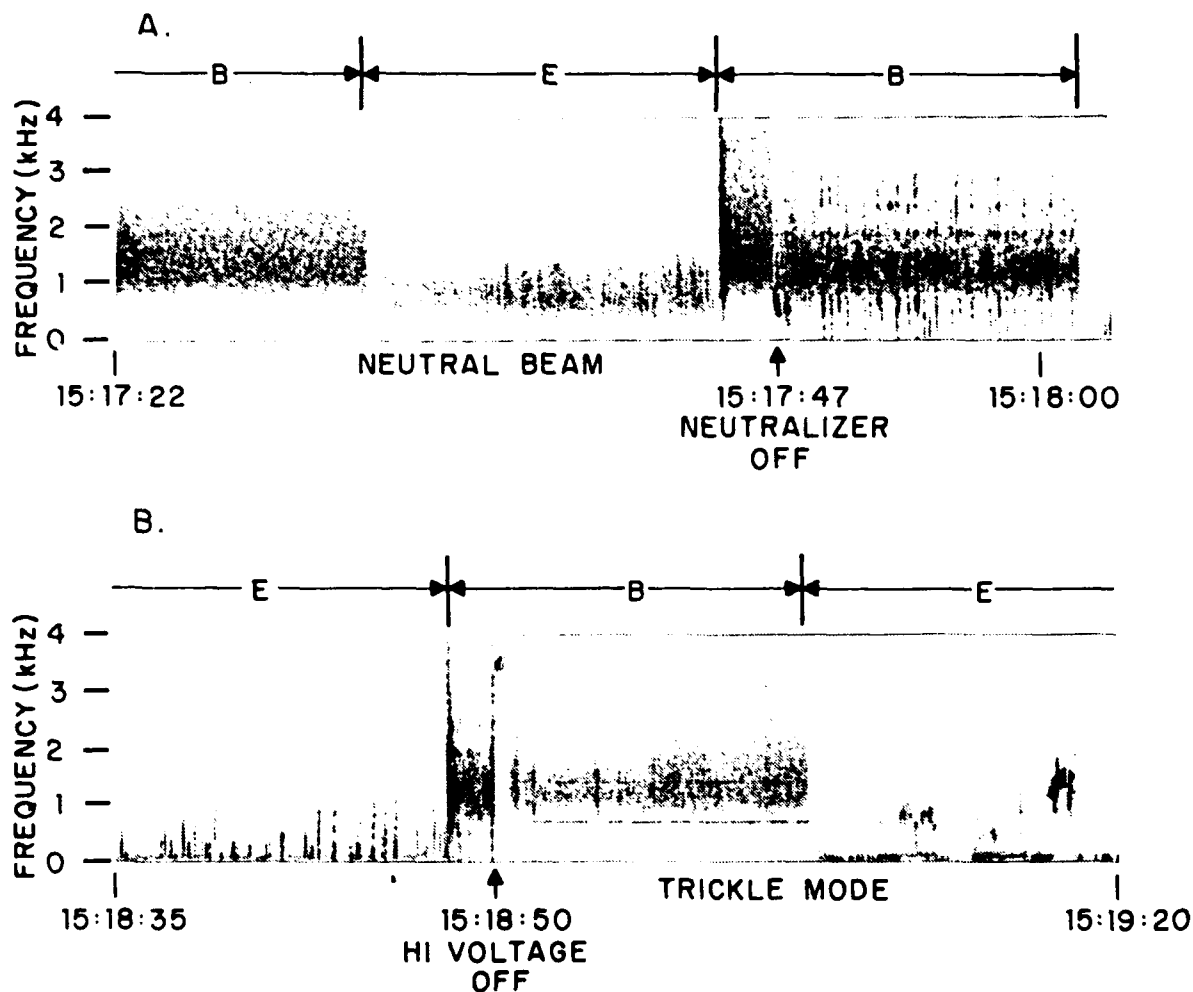## 2 April 1979

A.

B.

Figure 10. A) Plasma Wave Data, Wideband, Day 92. Neutralized ion
beam at 1 kV ions, 1.0 mA beam, 1.2 A neutralizer
current. Neutralizer bias is -100 V. Neutralizer off
at 15:17:47.

B) Plasma Wave Data, Wideband, Day 92. Nonneutral beam
at 1 kV ions, 1.0 mA initially. HV off at 15:18:50.

These data demonstrate that the arcing behavior is external to the ion gun, since the gun voltages are all on for the neutralized beam experiments. The absence of arcing during trickle mode, as well, shows the spiky behavior in the wideband data must correspond to arcing on the satellite surface.

Figure 11 shows the electric and magnetic field amplitudes corresponding to these spectra. The 16-second antenna cycling pattern is apparent here, as in the spectrograms. The 3 kHz and 400 hz data are shown in the top two panels and are representative of the other channels. The nominal beam and neutralizer settings are plotted below. Note that there is an imbalance in the emitted currents of 10 to 100 μA (e.g., a few %), which results in net negative charging. The neutralized beam (≈ first 2 minutes) results in a relatively high noise level in the 3 kHz magnetic loop (small boxes). The 3 kHz noise level drops when the neutralizer is switched off and the amplitude drops again when the beam voltage is switched off. The sequence is inverted as the beam voltage is first switched on, then the neutralizer. The behavior of the 400 Hz data differ in that the highest noise level occurs for the beam on but neutralizer off. This corresponds to the arcing period. The electric channel only responds at the lower frequencies, with virtually zero response above 3.0 kHz. There was not a 100 kHz response during trickle mode, in contrast to observations on 19 July 1979 (Figure 3).

Finally, Figure 11 shows the SC10 and SC11 data in the bottom two panels. The SC10/11 data are recorded for 0.1 to 1.0 Hz, 1.0 to 2.0 Hz, 2.0 to 20.0 Hz, and 20 to 200 Hz. Data are shown for the 2 to 20 Hz and 20 to 200 Hz channels. The solid line (with dots) shows the electric antenna data; the small boxes are the magnetometer data. At low frequencies (0.1 to 20 Hz) little or no signal is found in the magnetic field data. The electric channels are near zero (background) during trickle mode. In the 20 to 200 Hz data, slightly different behavior is found. The magnetometer data show a sharp increase during trickle mode, and the electric data remain above background. This increase in the 20 to 200 Hz magnetometer output is similar to that shown for 19 July 1979. The electric channel 20 to 200 Hz response is larger and is spin modulated.

D. SUMMARY OF OBSERVATIONS AND ANALYSIS

Broadband and narrowband wave data taken during the ion gun operations conducted throughout 1979 were surveyed. Data presented herein were chosen to show typical responses observed in the complete survey. Plasma wave response to ion gun operations showed little dependence on satellite location within the magnetosphere or environmental considerations

The major feature which was observed in the magnetic antenna data, for trickle mode, neutralized beams, and nonneutralized beams, was a broad peak from 1.0 to 1.5 kHz, which represents the white noise response of the receiver (Figures 5, 6A, 7, and 8A). The common feature in these cases is the mixture of a relatively cold, dense plasma with hot, tenuous plasma. (Also, the dense plasma is spatially limited.) The apparent current dependence of the broad peak (Figure 9) is presumably tied to the change in beam-limiting processes. It may be that space-charge oscillations outside the beam aperture are one source of the observed broadband signals.

The nonneutralized beam experiments result in satellite potentials approaching a kilovolt, and apparently arcing on the satellite surface. This interpretation of the observations is reinforced by the disappearance of the arcing signature (temporally narrow, wide-frequency range pulses) when the neutralizer was turned on, or when the beam accelerating voltage was switched off. The amplitude of the signals generated by these arcs was lower than those induced during natural charging events[3] (H. Koons, private communication). These arcs did not generate pulses which were large enough to trigger the arc discharge monitor. The decrease in the arcing signature as the beam current was reduced (Figure 8) may be the result of changes in the gain (AGC) driven by the increase in the steady white noise spectrum, or other beam driven features.

The accelerated beam produced a distinct signal in addition to the white noise background. This was the lower frequency peak, most apparent in the electric antenna below 1 kHz. The two main cases are illustrated in Figure 12. For the nonaccelerated beam (particularly trickle mode), Figure 12A shows the distribution function for the plasma near the satellite.

31

Figure 11. (Opposite Page) Electric and Magnetic Field Amplitudes
Corresponding to SCATHA Spectra. Top two panels show
plasma wave data from SC1, 400 Hz, 3.0 kHz. The magnetic
field data are shown with small boxes; the electric field
data with dots and lines. Note the alternation in antenna
at 16 s intervals.

Middle two panels Show SC10/11 data at 2.0 to 20.0 Hz and
20.0 to 200 Hz. Solid lines are electric antenna (SC10),
boxes are magnetometer data (SC11).

Bottom three panels: indicate the gun parameter settings.

32
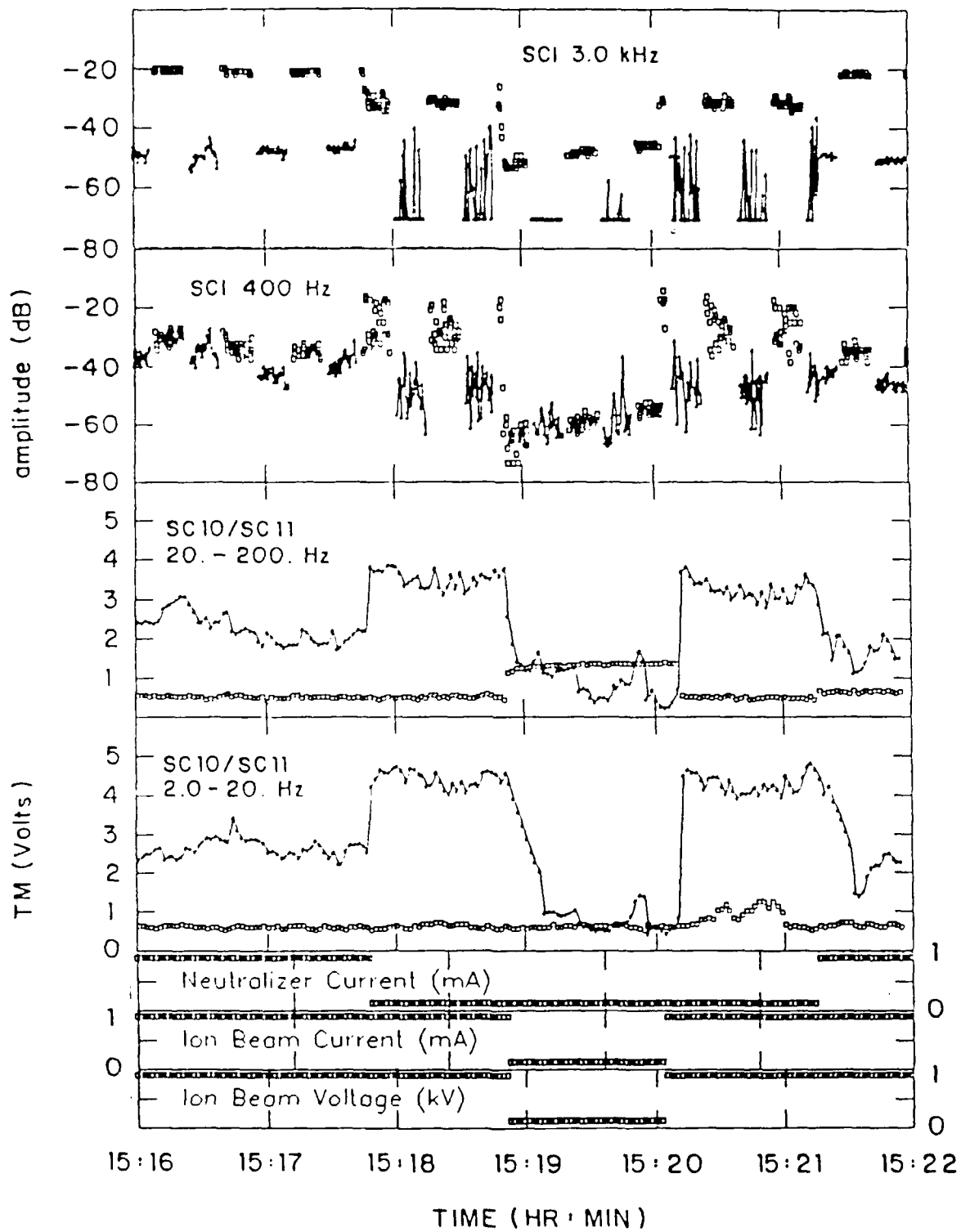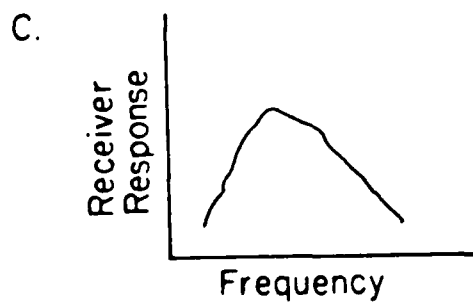
SCATHA
2 APRIL 1979
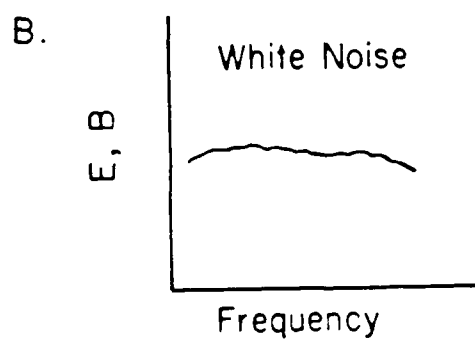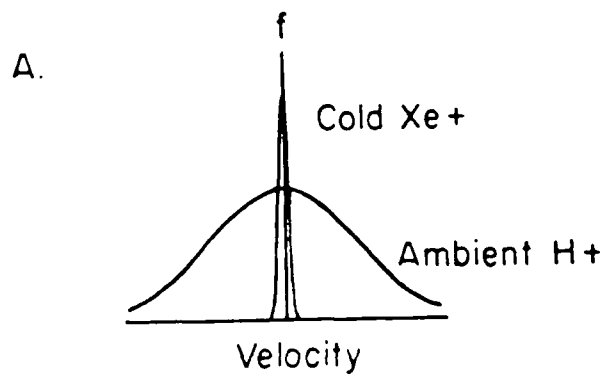

Figure 11

Figure 12. (Opposite Page) Cartoon Sketch of Plasma Conditions, Plasma Wave Signals, and Receiver Response.

A) The curves are intended to represent Maxwellian distributions centered at $V=0$. Parameters are H^+: $n = 8$ cm^{-3}, $T = 5$ eV; Xe^+: $N = 0.002$ cm^{-3}, $T = 2$ eV. The extremely narrow distribution for the Xe^+ is due to the relatively high mass (131 amu). The Xe^+ density is artificially low in order to keep the central distribution on scale. A more realistic density for trickle mode is 10-100 cm^{-3}.

B) Both the electric (E) and magnetic (B) spectra are inferred to be relatively flat.

C) The receiver response is peaked in the 1-1.5 kHz frequency range.

D) The 1 keV xenon beam results in a "beam-like" distribution in the H^+ reference frame. Parameters are $H+$: $n = 7.0$ cm^{-3}, $T = 5.0$ eV; Xe^+: $n = 0.0015$ cm^{-3}. $T = 2.0$ eV, $V = 38$ km/s. The xenon density in the beam would be orders of magnitude higher, and near the beam it might be more appropriate to consider the local H^+ to be a perturbation on the tail of the xenon distribution.

E) The white noise background is supplemented by an (inferred) ion-acoustic mode.

F) The receiver response with a distribution peaked at low frequencies.

34

MIXED PLASMA CLOUDS   BEAM IN PLASMA

A.
f

Cold Xe+

Ambient H+

Velocity

D.
f

Xe+
Beam

Ambient H+

Velocity

B.

White Noise

E, B

Frequency

E.

White Noise +
Ion Acoustic Mode

E, B

Frequency

C.

Receiver
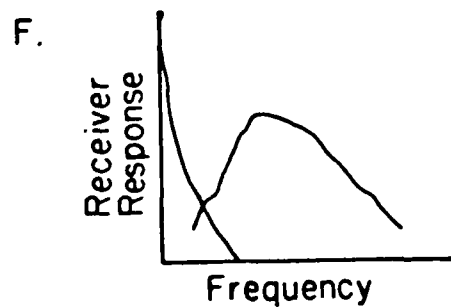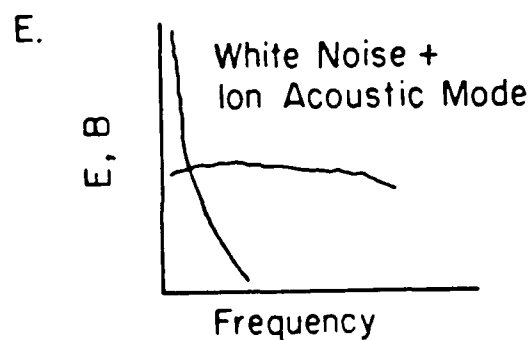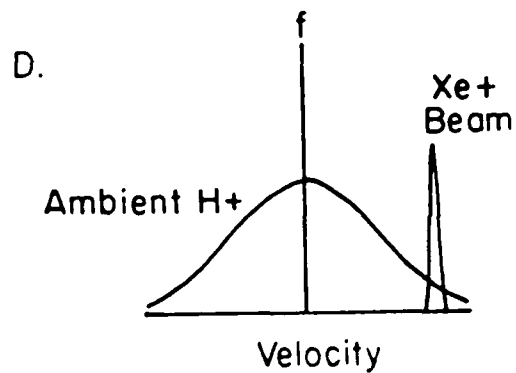Response

Frequency

F.

Receiver
Response

Frequency

Figure 12

35

Coincident with these (inferred) distributions, a white noise spectrum is generated by the discharge or the plasma distributions near the source, as sketched in Figure 12B. The receiver response (Figure 12C) is peaked at 1.0 to 1.5 kHz. The additional signal introduced by the (neutralized) beam is interpreted as the result of a beam in plasma distribution, as illustrated in Figure 12D. In addition to the combination of cold and hot plasmas, there is an offset in the beam center which may be sufficient to result in a positive slope distribution. Such distributions are unstable to waves such as the ion acoustic mode, which would have a frequency distribution similar to that shown in Figure 12E.[28,29] This would be combined with the white noise background for the receiver response illustrated in Figure 12F.

The growth rate for instabilities such as the ion-acoustic mode depend upon basic parameters such as the beam temperature and density, relative to the ambient parameters. It is likely that both the white noise response of the receivers, and the response to the low frequency beam-produced modes, can be explained by a detailed analysis of the appropriate beam-plasma dispersion relations. Such a treatment is substantially beyond the scope of the present work.

During trickle mode operations, the white noise signal is observed only on the magnetic antenna, which is physically close to the satellite. The electric antenna observes primarily natural signals. Examination of narrow-band filter data for this mode shows that input to the electric field antenna at 30 kHz and below is at "gun off" background levels, while the magnetic field antenna is still receiving signals with amplitude 20 - 30 dB above background. Hence, in general, trickle mode operations do not interfere with plasma wave observations on the long electric field antenna.

Trickle mode operations did produce two sets of signals unique to this mode. These were the 100 kHz signals seen in the electric antenna and the 20 - 200 Hz signals seen in the SC10 and SC11 data. The 100 kHz signals, seen only during the first example, would be consistent with electron plasma frequency or upper hybrid resonance signals if the ambient plasma density is about 100 cm^3. This is a reasonable value, given a nominal trickle model

current of 40 μA, moving outward due to a positive spacecraft potential of a few volts through a surface area of 10 to 100 m^2. The dimensions of the plasma cloud are comparable to the wavelength, which might be expected for this frequency (e.g., 30 m for an index of refraction of 100). The lack of this feature in the second data set presented here could be due to fairly small variations in the plasma density, since the passband is fairly narrow (±7.5%). A variation in total electron density of 15% would move the signal out of the 100 kHz channel. Minor variations in gun performance could have this effect. Also it is possible that variations in the nature of the ambient plasma could affect the amplitude of the signal, as with signals which are observed in the unperturbed plasmasphere.[30]

The signal in the 20 - 200 Hz band is appropriate for ion (H^+) Bernstein waves, the lower hybrid resonance, or perhaps xenon (Xe^+) plasma waves. The ambient plasma is from the plasma sheet, with a normal density of 1 cm^3, and keV temperature. The ion composition of the plasma sheet is variable, but is primarily H^+, with 10 to 50% O^+. Hence, the plasma environment around the satellite is primarily a Xe^+/electron plasma, with H^+ (or O^+) a minority constituent. If we assume a local density of 100 cm^{-3}, we obtain a xenon plasma frequency of ~ 180 Hz. If we use the measured magnetic field from the first event (80 γ), the lower hybrid resonance would be ~ 4 Hz for a xenon plasma, or ~ 50 Hz for an H^+ plasma. The gyrofrequencies are low, but ion Bernstein modes extend from f_{ci} to f_{LHR}. The most likely mode, from a frequency standpoint, is either the Xe^+ plasma wave or H^+ Bernstein mode.

The spin modulation of the electric antenna data seen most clearly in the second example (Figure 11) is similar to that found during observations of naturally occurring ion Bernstein waves (equatorial noise) with the same instrument[31] This indicates a dependence on magnetic aspect, which reflects wave polarization. The data from the magnetometer are taken from the axis parallel to the spin axis and hence are not spin modulated.

The intense low frequency (<100 Hz) signals normally found in the SC 1 electric antenna data (Figure 4B) disappeared during neutralized beam operations and some trickle mode operations. If this is not purely an AGC

effect, it could be the result of shielding of the antenna from spacecraft-generated noise. This would be analogous to the shielding of the DE-1 antenna from solar array noise observed in the plasmasphere.[30]

III. CONCLUSIONS

The ion beam experiments on SCATHA produced a variety of plasma wave phenomena. Arcing signatures were identified which can now be clearly associated with arcs on the satellite surface, not in the ion gun. This conclusion results from the disappearance of the arcing signature in trickle mode, when the full gas discharge is still operating, and the disappearance of the arcing signature when the beam is neutralized.

An intense white noise is generated near the satellite, which only couples weakly to the long electric antenna. This noise is largely independent of the gun mode. There is a lower frequency signal which is observed only when an accelerated beam is emitted.

Trickle model operations appeared to be relatively benign, in terms of interference with the natural plasma wave data. In fact, such operations offer the possibility of shielding plasma wave antenna from spacecraft-generated signals. This is significant since this mode is close in its operational results to the behavior of a hollow cathode gas discharge, which is a primary design for future satellite potential control applications.

REFERENCES

1. D. A. McPherson, D. P. Cauffman, and W. Schober, "Spacecraft Charging at High Altitudes - The SCATHA Satellite Program," paper presented at the AIAA 13th Aerospace Sciences Meeting, Pasadena, CA, AIAA 75-92 (January 20-22, 1975).

2. D. A. McPherson and W. R. Schober, "Spacecraft Charging at High Altitudes: The SCATHA Satellite Program," in Spacecraft Charging by Magnetospheric Plasma, Progress in Aeronautics and Astronautics, Vol. 47, ed. A. Rosen, IAA, pp. 15-30 (1976).

3. H. C. Koons, P. F. Mizera, J. L. Roeder, and J. F. Fennell, "Severe Spacecraft-Charging Event on SCATHA in September 1982," J. Space Rockets, 25, 239-243 (1988).

4. R. E. Hunter, R. O. Bartlett, R. M. Worlock, and E. L. James, "Cesium Contact Ion Microthruster Experiments Onboard Applications Technology Satellite (ATS)-IV," J. Spacecraft Rockets, 6, 968-970 (1969).

5. R. C. Olsen, "Experiments in Charge Control at Geosynchronous Orbit - ATS-5 and ATS-6," J. Spacecraft Rockets, 22, 254-264 (1985).

6. W. R. Kerslake and R. C. Finke, "SERT II Spacecraft Thruster Restart - 1974," J. Spacecraft Rockets, 12, 780-782 (1975).

7. W. R. Kerslake and S. Domitz, "Neutralization Tests on the SERT II Spacecraft," reprint from Princeton/AIAA/DGLR 14th International Electric Propulsion Conference, Princeton, N. J., AIAA 79-2064 (Oct. 30-Nov. 1, 1979).

8. P. M. Kintner and M. C. Kelley, "Ion Beam Produced Plasma Waves Observed by the Delta n/n Plasma Wave Receiver During the Porcupine Experiment," in Advances in Space Research, Active Experiments in Space Plasmas, Vol. 1, No. 2, pp. 107-115, ed. C. T. Russell and M. J. Rycroft, Pergamon Press Ltd., Oxford, England (1981).

9. P. M. Kinter and M. C. Kelley, "Plasma Waves Produced by the Xenon Ion Beam Experiment on the Porcupine Sounding Rocket," in Artificial Particle Beams in Space Plasma Studies, pp. 199-205, ed. B. Grandal, Plenum Press New York, pp. 199-205 (1982).

10. R. L. Kaufmann, D. N. Walker, J. C. Holmes, C. J. Pollock, R. L. Arnoldy, L. J. Cahill, and P. M. Kintner, "Heavy Ion Beam-Ionosphere Interactions: Charging and Neutralizing the Payload," J. Geophys. Res., 94, 453-471 (1989).

11. T. E. Moore, R. L. Arnoldy, R. L. Kaufmann, J. J. Cahill, P. M. Kintner, and D. N. Walker, "Anomalous Auroral Electron Distributions Due to an Artificial Ion Beam in the Ionosphere," J. Geophys. Res., 87, 7569-7579 (1982).

12. D. Jones, "Xe$^+$-Induced Ion-Cyclotron Harmonic Waves," in Advances in Space Research, Active Experiments in Space Plasmas, Vol. 1, No. 2, pp. 103-106, ed. C. T. Russell and J. J. Rycroft, Pergamon Press Ltd., Oxford, England (1981).

13. P. M. Kintner and M. C. Kelley, "A Perpendicular Ion Beam Instability: Solutions to the Linear Dispersion Relation," J. Geophys. Res., 88, 357-359 (1983).

14. B. R. A. Häusler, O. H. Bauer, G. Haerendel, R. Bush, C. W. Carlson, B. Theiler, M. C. Kelley, V. S. Dokukin, and Y. Y. Ruzhin, "Observations of the Artificially Injected Porcupine Xenon Ion Beam in the Ionosphere, J. Geophys. Res., 91, 287-303 (1986).

15. R. Pottelette, J. M. Illiano, O. H. Bauer, and R. Treumann, "Observation of High-Frequency Turbulence Induced by an Artificial Ion Beam in the Ionosphere," J. Geophys. Res., 89, 2324-2334 (1984).

16. J. Thiel, R. O. Storey, O. H. Bauer, and D. Jones, "Excitation of the Lower Oblique Resonance by an Artificial Plasma Jet in the Ionosphere," J. Geophys. Res., 89, 2385-2387 (1984).

17. D. N. Walker, "Perpendicular Ion Beam-Driven Instability in a Multi-component Plasma: Effects of Varying Ion Composition on Linear Flute Mode Oscillations," J. Geophys. Res., 91, 3305-3310 (1986).

18. M. K. Hudson and I. Roth, "Thermal Fluctuations from an Artificial Ion Beam Injection into the Ionosphere," J. Geophysical Res., 89, 9812-9822 (1984).

19. R. E. Erlandson, L. J. Cahill, C. J. Pollock, R. L. Arnoldy, W. A. Scales, and P. M. Kintner, "Initial Results from the Operation of Two Argon Ion Generators in the Ionosphere," J. Geophys Res., 92, 4601-4616 (1987).

20. I. Kudo, K. Machida, H. Murakami, and Y. Toda, "Electromagnetic Noise from an Ion Engine System," J. Spacecraft Rockets, 20, 84-88 (1983).

21. H. C. Koons and H. A. Cohen, "Plasma Waves and Electrical Discharges Stimulated by Beam Operations on a High Altitude Satellite," in Artificial Particle Beams in Space Plasma Studies, ed. B. Grandal, Plenum Press, New York, pp. 111-120 (1982).

22. L. E. Weddle, "Ion Gun Generated Electromagnetic Interference on the SCATHA Satellite," Masters Thesis, Naval Postgraduate School (1987).

23. G. Haerendel and R. Z. Sagdeev, "Artificial Plasma Jet in the Ionosphere," in Advances in Space Research, Active Experiments in Space Plasmas, Vol. 1, No. 2, pp. 29-46, ed. C. T. Russell and M. J. Rycroft, Pergammon Press Ltd., Oxford, England (1981).

24. I. Roth, C. W. Carlson, M. K. Hudson, and R. L. Lysak, "Simulation of Beam Excited Minor Species Gyroharmonics in the Porcupine Experiment," J. Geophys. Res., 88, 8115-8122 (1983).

25. J. F. Fennell, "Description of P78-2 (SCATHA) Satellite and Experiments," in IMS Source Book, pp. 65-78, AGU, Washington, DC (1982).

26. T. D. Masek and H. A. Cohen, "Satellite Positive-Ion-Beam System," J. Spacecraft Rockets, 15, 27-33 (1978).

27. P. Werner, "Ion Gun Operations at High Altitudes," Masters Thesis, Naval Postgraduate School (1988).

28. F. F. Chen, Introduction to Plasma Physics and Controlled Fusion, 2nd ed., Vol. 1, pp. 95-98, 267-273, Plenum Press (1984).

29. B. B. Kadomtsev, Plasma Turbulence, Translated by L. C. Ronson, ed. M. G. Rusbridge, pp. 35-39, Academic Press, New York (1965).

30. R. C. Olsen, S. D. Shawhan, D. L. Gallagher, J. L. Green, C. R. Chappell, and R. R. Anderson, "Plasma Observations at the Earth's Magnetic Equator," J. Geophys Res., 92 2385-2407 (1987).

31. R. C. Olsen, "Equatorially Trapped Plasma Populations," J. Geophys. Res., 8, 11235-11245 (1981).

LABORATORY OPERATIONS

The Aerospace Corporation functions as an "architect-engineer" for national security projects, specializing in advanced military space systems. Providing research support, the corporation's Laboratory Operations conducts experimental and theoretical investigations that focus on the application of scientific and technical advances to such systems. Vital to the success of these investigations is the technical staff's wide-ranging expertise and its ability to stay current with new developments. This expertise is enhanced by a research program aimed at dealing with the many problems associated with rapidly evolving space systems. Contributing their capabilities to the research effort are these individual laboratories:

Aerophysics Laboratory: Launch vehicle and reentry fluid mechanics, heat transfer and flight dynamics; chemical and electric propulsion, propellant chemistry, chemical dynamics, environmental chemistry, trace detection; spacecraft structural mechanics, contamination, thermal and structural control; high temperature thermomechanics, gas kinetics and radiation; cw and pulsed chemical and excimer laser development, including chemical kinetics, spectroscopy, optical resonators, beam control, atmospheric propagation, laser effects and countermeasures.

Chemistry and Physics Laboratory: Atmospheric chemical reactions, atmospheric optics, light scattering, state-specific chemical reactions and radiative signatures of missile plumes, sensor out-of-field-of-view rejection, applied laser spectroscopy, laser chemistry, laser optoelectronics, solar cell physics, battery electrochemistry, space vacuum and radiation effects on materials, lubrication and surface phenomena, thermionic emission, photosensitive materials and detectors, atomic frequency standards, and environmental chemistry.

Electronics Research Laboratory: Microelectronics, solid-state device physics, compound semiconductors, radiation hardening; electro-optics, quantum electronics, solid-state lasers, optical propagation and communications; microwave semiconductor devices, microwave/millimeter wave measurements, diagnostics and radiometry, micro-wave/millimeter wave thermionic devices; atomic time and frequency standards; antennas, rf systems, electromagnetic propagation phenomena, space communication systems.

Materials Sciences Laboratory: Development of new materials: metals, alloys, ceramics, polymers and their composites, and new forms of carbon; nondestructive evaluation, component failure analysis and reliability; fracture mechanics and stress corrosion; analysis and evaluation of materials at cryogenic and elevated temperatures as well as in space and enemy-induced environments.

Space Sciences Laboratory: Magnetospheric, auroral and cosmic ray physics, wave-particle interactions, magnetospheric plasma waves; atmospheric and ionospheric physics, density and composition of the upper atmosphere, remote sensing using atmospheric radiation; solar physics, infrared astronomy, infrared signature analysis; effects of solar activity, magnetic storms and nuclear explosions on the earth's atmosphere, ionosphere and magnetosphere; effects of electromagnetic and particulate radiations on space systems; space instrumentation.